An IoT LoRaWAN Network for Environmental Radiation Monitoring

L. Gallego Manzano, Hamza Boukabache, *Member, IEEE*, Salvatore Danzeca, Natalie Heracleous, Fabrizio Murtas, Daniel Perrin, Vasja Pirc, Alejandro Ribagorda Alfaro, Alessandro Zimmaro, and Marco Silari

***Abstract*— A reliable and highly scalable Internet of Things (IoT) end-to-end data infrastructure has been developed for environmental radiation monitoring at the European Organization for Nuclear Research (CERN) based on a low-power wide-area network (LPWAN). The proposed system, called Waste radiation MONitoring (W-MON), consists of an interconnected network of thousands of highly sensitive and ultralow-power gamma radiation sensors acting as long range (LoRa) transceivers. The aim of the system is to improve and automatize the radiological controls of conventional waste containers. The end devices measure the radiation levels in the waste containers on a continuous basis and send the data periodically to the LoRaWAN network server. The network has been deployed in an outdoor environment covering hundreds of hectares. A set of web-based user applications for real-time monitoring, data visualization, and status control of the devices have been designed based on open-source tools. The data pipeline infrastructure has been designed to allow an easy integration into the overall CERN Radiation and Environment Monitoring Unified Supervision service (REMUS).**

***Index Terms*— Environmental radiation monitoring, Internet of Things (IoT), long range (LoRa), low-power wide-area network (LPWAN), radioactive waste monitoring.**

I. Introduction

In THE field of radiation protection, environmental radiation monitoring is essential to control the exposure to ionizing radiation and to protect the people and the environment from potential radiation hazards. In particular, radiation monitoring of waste is a key aspect of radiation protection in organizations, such as the European Organization for Nuclear Research (CERN). To ensure that no radioactive material accidentally ends up mixed with ordinary waste that leaves the CERN sites, the Radiation Protection Group has set a multilevel radiological monitoring strategy of conventional waste. The first-level control consists in the routine monitoring of waste containers by radiation protection technicians equipped with a handheld radiation survey meter. In order to overcome the limitations of a manual radiological survey (gaps in sensitivity, burdensome and taxing job, no time-stamped measurements, and so on), the Waste radiation MONitoring (W-MON) project [1] proposes a distributed Internet of Things (IoT) network for environmental radiation monitoring, which consists of smart, sensitive, and compact gamma radiation detectors with periodic wireless data transmission for real-time monitoring of the radiation levels in standard waste containers. The system has been specifically designed for the detection of very low radioactive levels above the natural background (around 100 nSv/h), providing identification and early warning of a possible radiation release event.

The IoT has allowed the connection of conventional measuring devices to the Internet, providing smart solutions to daily-based problems [2]. In fact, the deployment of IoT networks had an impact on numerous applications, such as smart cities, transportation, healthcare [3]–[6]. IoT applications for environmental and ambient monitoring of large areas have been studied in [7]–[9]. In particular, the use of smart sensors with IoT connectivity has shown its potential for improved waste management and monitoring systems [10]–[12]. IoT has also been proposed for monitoring applications based on radiation sensors, mainly for radiation surveillance in nuclear power plants [13], [14]. The system proposed in this article benefits from the potential of IoT networks to monitor large areas [15] for the radiological control of waste containers. To our knowledge, this article presents for the first time a distributed network for real-time remote monitoring of radioactivity in metallic waste containers. It is also the first to evaluate the effects of a metallic waste container on packet reception efficiency.

The proposed IoT infrastructure incorporates a low-power wide-area network (LPWAN) that uses long range (LoRa) technology, enabling a large-area low-power IoT deployment [15], [16]. The system follows the standards and protocols of an IoT LoRaWAN architecture. It has been designed to cover a wide area of hundreds of hectares with thousands of sensors working simultaneously for several years. The sensors provide stable long-term low-dose-rate measurements under demanding operating conditions [1]. The radiation levels are

Manuscript received January 3, 2021; revised April 25, 2021; accepted May 26, 2021. Date of publication June 16, 2021; date of current version July 9, 2021. The Associate Editor coordinating the review process was Dr. Sabrina Grassini. *(Corresponding author: L. Gallego Manzano.)*

L. Gallego Manzano is with the European Organization for Nuclear Research (CERN), 1211 Geneva, Switzerland, and also with the Institute of Radiation Physics, Lausanne University Hospital and University of Lausanne, 1007 Lausanne, Switzerland (e-mail: lucia.gallego-manzano@chuv.ch).

Hamza Boukabache, Salvatore Danzeca, Natalie Heracleous, Daniel Perrin, Vasja Pirc, Alessandro Zimmaro, and Marco Silari are with the European Organization for Nuclear Research (CERN), 1211 Geneva, Switzerland.

Fabrizio Murtas is with the European Organization for Nuclear Research (CERN), 1211 Geneva, Switzerland, and also with Frascati National Laboratories, Italian Institute for Nuclear Physics (INFN), 00044 Frascati, Italy.

Alejandro Ribagorda Alfaro is with Advanced Oncotherapy plc, 1217 Meyrin, Switzerland.

Digital Object Identifier 10.1109/TIM.2021.3089776

periodically transmitted to the LoRa server and stored in a database with a detailed event log. A set of web-based user applications with graphic controls for real-time data visualization have been designed based on open-source tools. The IoT end-to-end data infrastructure has been tested for over a year showing stable and reliable operation. The next step will be the final integration into the overall CERN Radiation and Environment Monitoring Unified Supervision service (REMUS) [17].

The goal of this article is to provide a detailed description of the W-MON IoT infrastructure and the evaluation of the CERN LoRa network within the scope of the W-MON project. This article is organized as follows. In Section II, the CERN LoRaWAN network is described for the first time and the overall W-MON IoT system architecture is presented. The end devices are described in Section III. Sections IV and V include the implementation of the radiation sensor network and the results in terms of signal quality, signal-to-noise ratio (SNR), and packet reception ratio (prr; i.e., the percentage of transmitted packets that are successfully received by the server) at different locations and experimental configurations. Finally, the conclusions and future steps are summarized in Section VI.

II. W-MON Wireless Communication Technology: Why LoRa?

Currently, the radiological controls need to be performed over more than 200 containers for ordinary waste, located outside buildings where there is a risk of accidental disposal of radioactive material (e.g., close to accelerator access points). This implies that the containers are distributed over a wide area covering hundreds of hectares. The containers are placed outdoors, surrounded by buildings and, occasionally, by heavily shielded facilities. Extensive tests and simulations showed that the best sensor arrangement implies eight sensors per container in order to provide full coverage of the inner volume with the required sensitivity while ensuring cost-effectiveness (see [1] for details). Consequently, due to the large number of devices and the scale and diversity of deployments, the wireless technology used for the W-MON IoT infrastructure needs to be cost-effective and provide wide coverage. The signals should be able to penetrate buildings and coexist with many other devices. Moreover, the sensors must be battery-powered and operate for several years with minimal maintenance.

Based on these requirements, data transmission and communication from the sensors to the monitoring system is achieved via an LPWAN technology [18], [19], in particular, via LoRa that provides long-range (around 2 km in dense urban areas and up to 15 km in rural areas) low-power wireless communication [16], [20], [21]. Alternatives, such as Wi-Fi and Low-Energy Bluetooth, were discarded due to either high power consumption or limited range. The characteristics of LoRa in terms of low power and LoRa make it the best option for wireless data transmission where small amounts of data need to be sent regularly over a wide area. Moreover, LoRa is designed to potentially serve millions of devices operating at low data rates [22], suiting the needs of W-MON where

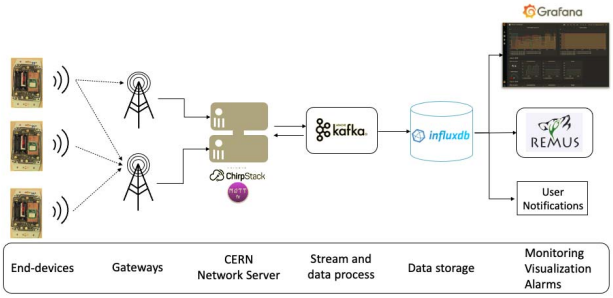

Fig. 1. W-MON IoT LoRaWAN architecture.

thousands of devices are expected to work simultaneously. Nevertheless, the scalability of the network can be seriously affected by the duty-cycle restrictions imposed by frequency regulations and concurrent LoRa transmissions, which could lead to a potential signal loss or substantial delays [23]–[26].

In the early stages of the project, two alternative models were considered for data transmission. In the first one, each individual sensor in the waste container acted as a LoRa transceiver sending data to the central server. The second alternative was based on a master–slave model; seven of the eight individual sensors per container, i.e., slaves, sent the data to the eighth unit that acted as a master collecting all the information for subsequent transfer to the server. The latter was proposed to reduce the number of devices sending data simultaneously and, therefore, reduce the potential number of collisions [27]. Here, data transmission between slaves and master does not need to be LoRa, and hence, among the different available wireless technologies, Wi-Fi was chosen for simplicity [28], [29]. Several parameters were analyzed to assess the most suited communication model. The results are presented in Section IV.

A. System Architecture and Design

The W-MON IoT infrastructure, shown in Fig. 1, relies on two types of devices: the end devices or nodes, arranged in arrays of eight devices per container, and the gateways. The end devices consist of an autonomous battery-powered gamma radiation sensor coupled with specifically designed hardware for LoRa data transmission and communication. The devices have been programmed to send small amounts of data periodically to the LoRaWAN network server (LNS) (see Section III). Gateways are intermediate devices that act as a bridge between the end devices and the network, receiving the data from each end device and forwarding them to the network server. Typically, there is no exclusive association between nodes and gateways, but the same uplink message can be received by several gateways within the range.

The CERN LNS is based on ChirpStack [30] and uses the Message Queuing Telemetry Transport (MQTT) protocol for communication [31]. The connectivity between the network server and the monitoring system ensures a secure data flow and high quality of service (QoS). The CERN LoRaWAN network communicates with Kafka [32] for real-time data streaming. Kafka is a scalable, high-throughput and distributed data streaming platform, which enables applications to be connected to each other. InfluxDB [33] is used as data storage for large amounts of time-stamped data, including DevOps

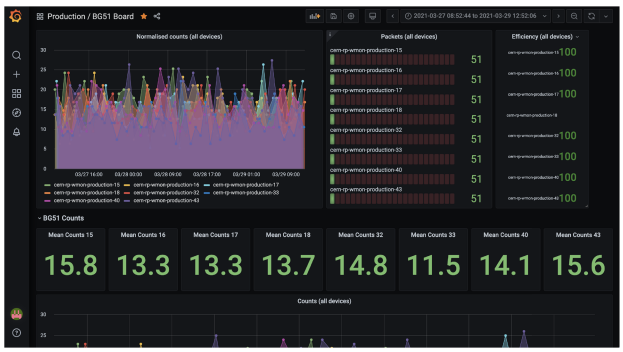

Fig. 2. Screenshot of the customized Grafana dashboard for the monitoring of one container with eight BG51 radiation sensors.

monitoring, log data, application metrics, IoT sensor data, and real-time analytics. Finally, a set of customized user dashboards for real-time monitoring, data visualization, and status control of the devices has been created using Grafana [34]. Grafana is a visualization platform with which interactive dashboards can be designed to query, visualize, and define levels of alerts on metrics and logs. An example dashboard for W-MON is shown in Fig. 2. It should be noted that decisions about the network and gateways were made based on a CERN-wide multipurpose network. The choice of technologies was based on their flexibility, scalability, and reliability in building robust real-time IoT applications. Hence, the new W-MON data infrastructure is a reliable and highly scalable monitoring architecture based on state-of-the-art open-source technologies and it has been designed to ensure and facilitate the final integration of the system into REMUS.

B. CERN LoRaWAN Network

The performance of LPWAN technologies makes them appropriate for large-scale outdoor deployments such as W-MON. LoRa networks have been successfully deployed in different environments, from indoor facilities and dense urban areas [35]–[37] to rural and sea scenarios for maritime communications [38]–[40]. Different deployments have shown their impact on connectivity range, coverage, and sensitivity.

For our specific application, the containers are located outdoors but in very diverse locations. Some of them are placed in a relatively open space without obstacles, allowing a high transmission range with a free line of sight between the sensors and gateways. In other cases, the containers are either surrounded by buildings or the line of sight is blocked by a heavily shielded facility that could affect the signal performance. Therefore, to ensure an efficient data transmission regardless of the location, CERN has deployed a new LoRaWAN network [41] with a strategic number of gateways mounted on the roof of several buildings. One of the gateways is, for example, installed on top of the water tower at a height of about 58 m, the highest point at CERN. The number of gateways was chosen to ensure coverage of every surface point and specific underground points at CERN. At the time of the tests, the CERN LoRa network consisted of ten outdoor gateways in order to cover the entire campus, including almost all areas on the two main CERN sites: Meyrin and Prévessin of 79 and 88 ha, respectively

TABLE I
LOCATION AND HEIGHT OF THE LoRa GATEWAYS

	Building	Height
Gateway A	227	58 m
Gateway B	60	28 m
Gateway C	157	indoors
Gateway D	866	11 m
Gateway E	2455	15 m

(see Fig. 3) and the large hadron collider (LHC) points. One additional gateway was installed indoors to serve other projects [42]. Some of the gateways relevant to these tests and their height are reported in Table I. Currently, the gateway deployment includes 17 additional indoor gateways to cover the LHC tunnel. It should be emphasized that the number of gateways can be easily increased to meet a greater capacity as may be required in the future. In particular, due to the increasing number of devices using LoRa, some extra outdoor gateways will be installed at critical locations on the Meyrin and Prévessin sites.

III. END DEVICES

The end devices consist of a highly sensitive and compact gamma radiation sensor allowing the detection of fluctuations above the natural background level and the measurement of gamma radiation dose rate over a wide energy range. Currently, three radiation sensors are under investigation: a customized version of the D-shuttle personal dosimeter developed in collaboration with the National Institute of Advanced Industrial Science and Technology (AIST) and Chiyoda Technol Corporation, the BG51 from Teviso Technologies, and the NI-RM02 developed by Nuclear Instruments [1]. The three sensors are sensitive and energy-efficient Si-based devices. The sensors have been calibrated in the CERN Radiation Calibration Facility [43], [44]. They have been programmed to detect count rate variations from background over a time scale of 1 h. Background measurements will be used to verify the stability of the sensors over time. Nonetheless, a complete calibration will be carried out at the moment of the battery exchange. Full details are given in [1].

The sensors are coupled to an ultralow-power electronic board with custom-designed hardware and software, allowing for long-range low-power LoRa wireless data transmission (see Fig. 4). The board has been designed to host different sensor types depending on the intended user case [42]. An intermediate printed circuit board (PCB) is required to connect each sensor to the communication board. Fig. 5 shows one of the gamma radiation sensors soldered onto the intermediate board and connected to the communication board. The LoRa transceiver includes an ATSAML21G18B microcontroller unit (MCU), an RFM95W-868S2 LoRa module operating in Class A mode, and an ANT-868-JJB-ST LoRa antenna. A conceptual diagram of the electronic board is shown in Fig. 6.

The firmware is designed to minimize the power consumption. Confirmed uplink (ACK) and downlink messages are implemented and can be easily enabled if needed. In case

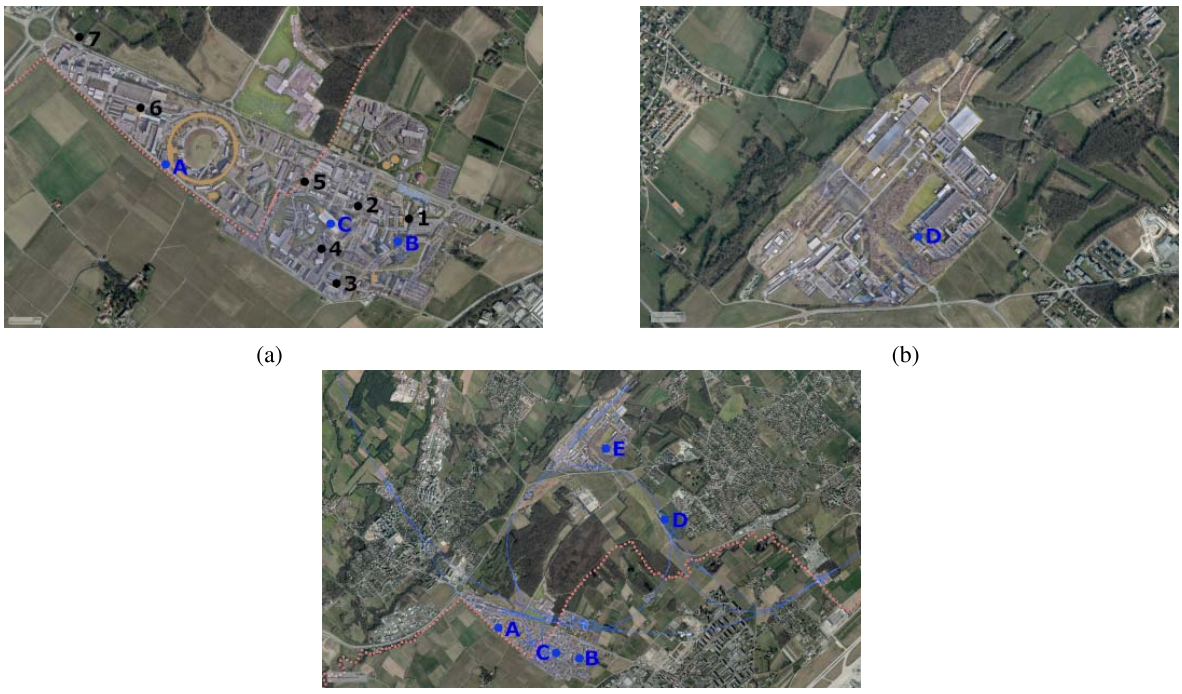

(a) (b) (c)

Fig. 3. Maps of the CERN (a) Meyrin and (b) Prévessin sites. (c) Part of the accelerator complex. The blue circles indicate the location of the LoRa gateways. The letters A, B, D, and E illustrate the position of the outdoor gateways, while the letter C shows the indoor LoRa gateway placed inside CHARM. The black circles in (a) show the seven test points.

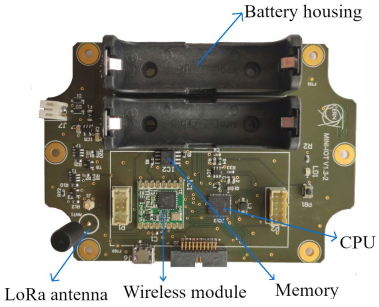

Fig. 4. Electronic board with LoRa data transmission.

Fig. 5. Customized D-shuttle radiation sensor soldered onto the intermediate board and connected to the communication board. The device is hosted in an IP67 plastic box.

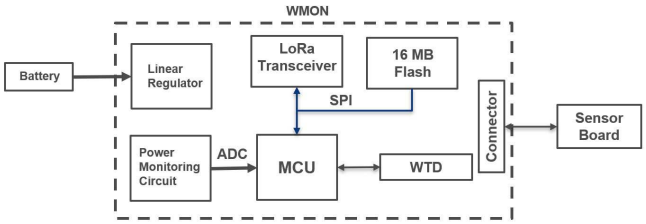

Fig. 6. Conceptual diagram of the electronic board.

of LoRaWAN downtime, data from the radiation sensors are stored in a flash onboard memory. The transmission time can be easily adjusted ensuring flexibility and adaptability to different scenarios. The payload size, on the other hand, is fixed at 41 bytes with 30 bytes of sensor data. It includes the hourly integrated counts for the past 3 h (this redundancy is used in order to ensure the continuity of the service), device ID, and power supply level. The 3.3-V value is used as an estimate of the power consumption and the residual battery lifetime. A high-dose threshold was set in the firmware to facilitate an early warning if a material with a count rate several times above the natural background is dumped in the container. The frequency with which this alarm threshold is checked can be easily modified. Currently, the alarm threshold is verified three times per hour. The nodes are battery-powered by two 3.6-V, 2.6-Ah lithium-thionyl chloride AA batteries. Each end device is housed in an IP67 plastic box (see Fig. 5) and mounted in the 800-L metallic containers for ordinary waste of dimensions 110 cm $\times$ 70 cm $\times$ 90 cm. Previous studies showed that the best sensor configuration includes two sensors at the bottom (mounted outside the container), in a central position; four sensors at mid height on the sidewalls, and two sensors on the lid (mounted inside the container) [1].

A. Power Consumption Analysis

The overall power consumption of the end devices depends on the radiation sensor, the LoRa settings, and the location

TABLE II
SETTINGS OF THE LoRa PARAMETERS FOR DIFFERENT CONFIGURATIONS

	Conf. 1	Conf. 2	Conf. 3	Conf. 4
Bandwidth	125 kHz	125 kHz	125 kHz	125 kHz
Spreading Factor (SF)	7	ADR[1]	ADR[1]	ADR[1]
Data rate	5	ADR[1]	ADR[1]	ADR[1]
Transmitted Power	14 dBm	14 dBm	14 dBm	14 dBm
Center-band Frequency	868 MHz	868 MHz	868 MHz	868 MHz
Coding rate	4/5	4/5	4/5	4/5
Data rate	1 hour	1 minute	1 hour	6 minutes
Payload size	22 bytes	41 bytes	41 bytes	41 bytes

[1] Adaptive data rate

of the devices and their proximity to a gateway. To test the power consumption performance, the devices were configured according to Conf. 4 in Table II. The 41-byte packets were sent every 6 min with an initial spreading factor (SF) of 8 (see Section IV for details about the LoRa physical layer). The alarm threshold was checked every 2 min. The current consumption profile for a whole measurement cycle using the customized D-shuttle is shown in Fig. 7. The firmware data flow is summarized in Fig. 8. In the first 2 s, the MCU wakes up and performs the system initialization. The initialization phase occurs only once in the operating time of the device. Afterward, the devices try to join the LoRa network. In this example, the LoRa initialization phase takes around 14 s. This time can vary between 1 and 60 s depending on the quality of the connection. If the connection does not succeed within 180 s, the device enters in sleep mode for 1 h. This cycle is repeated n-configurable times. After the third attempt, the devices will try to connect every 60 s instead of every 180 s. If the device does not succeed to connect after these n attempts, it enters in sleep mode for 2 h before retrying. Identical steps are followed if the network is not available before a transmission. The initialization and LoRa activation phases are represented by the label BOOT in Fig. 7. Once the connection is established, the end devices enter in sleep mode and start measuring the radiation levels. The time period that the device is in sleep mode is shown as *tsleep* in Fig. 8. The sleep current is around 142 μA. For the other two sensors, the sleep current while measuring is 192 μA and 207 μA for the NI-R02 and BG51, respectively. The power consumption of the end nodes in sleep mode is 16, 38, and 71 μA for the BG51, D-shuttle, and NI-R02, respectively. The higher overall energy consumption of the BG51 is due to the addition of an external shock sensor (three-axis digital accelerometer LIS331DLH from STMicroelectronics). The shock sensor is necessary to avoid spurious signals. Three sets of measurements are performed per transmission time window. For a 6-min window, measurements are carried out every 120 s. After each period of 120 s, the MCU wakes up, reads the counts from the radiation sensor, and checks whether the alarm threshold has been reached (note the sharp 1-mA peaks in Fig. 7). If so, the cycle is interrupted and an alarm is sent to the supervision system. In Fig. 7, no threshold has been triggered. At the end of the cycle, packets are sent via LoRa and the MCU goes back to sleep until the next measurement

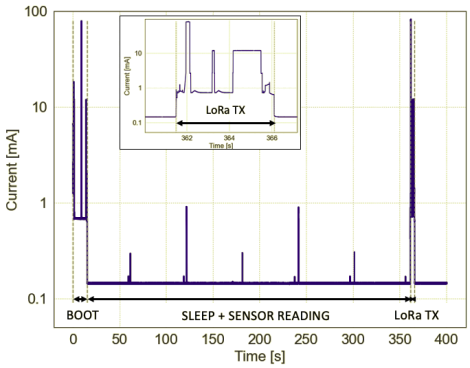

Fig. 7. Measured current consumption of a customized D-shuttle LoRa node over a 360-s cycle. The inside plot is a zoom on the LoRa transmission phase. The 1-mA spikes correspond to the periodic alarm checks. The low amplitude spikes correspond to the wake-up times of the external watchdog.

TABLE III
MEASURED CURRENT AND ENERGY CONSUMPTION OF A CUSTOMIZED D-SHUTTLE LoRa NODE FOR THE DIFFERENT PHASES OF THE DUTY CYCLE ASSUMING ONE LoRa TRANSMISSION PER HOUR

Process	$\bar{I}$ [mA]	Time [s]	Charge [μAh]
Boot	1.921	16	8.54
LoRa TX	8.481	4	9.42
Sleep	0.142	3596	141.84
Cycle	0.159	3616	159.80

period. The final cycle phase, which includes sensor data reading, alarm threshold check, LoRa data transmission, and data writing in the flash memory, takes around 4 s with an energy consumption of 9.42 μAh. After the LoRa transmission phase (LoRa TX in Fig. 7), the end devices enter again in sleep mode and start a new measurement cycle. The measured energy consumption per cycle for a 6-min data transmission is 32 μAh (see Fig. 9). Results for different measurement periods are summarized in Table III. We can see that the wireless LoRa transmission (LoRa TX) current consumption is negligible, whereas the sensor reading while in sleep mode contributes the most to the current consumption, being in any case low power consuming. The estimated power consumption for the three types of end devices per cycle and for 1-h measurement period is: 159.80, 207.29, and 221.08 μAh for the D-shuttle, NI-R02, and BG51, respectively. For two batteries of nominal capacity of 2.6 Ah and the standard W-MON data configuration (Conf.3 in Table II), which includes one 41-byte data transmission packet per hour, and assuming a simple linear battery model, we expect a battery lifetime of around 3.7 years for the D-shuttle, 2.9 years for the NI-R02, and 2.7 years for the BG51 radiation sensors.

IV. MASTER–SLAVE VERSUS ALL-MASTER MODEL

A first experiment was carried out in order to test the two communication models simultaneously: master–slave and all-master (see Section II). A pilot waste container was equipped with a fully operational monitoring system. The container integrated eight devices: three slaves and five masters (one for the master–slaves configuration). At the time of the test, the electronic board described in Section III was not

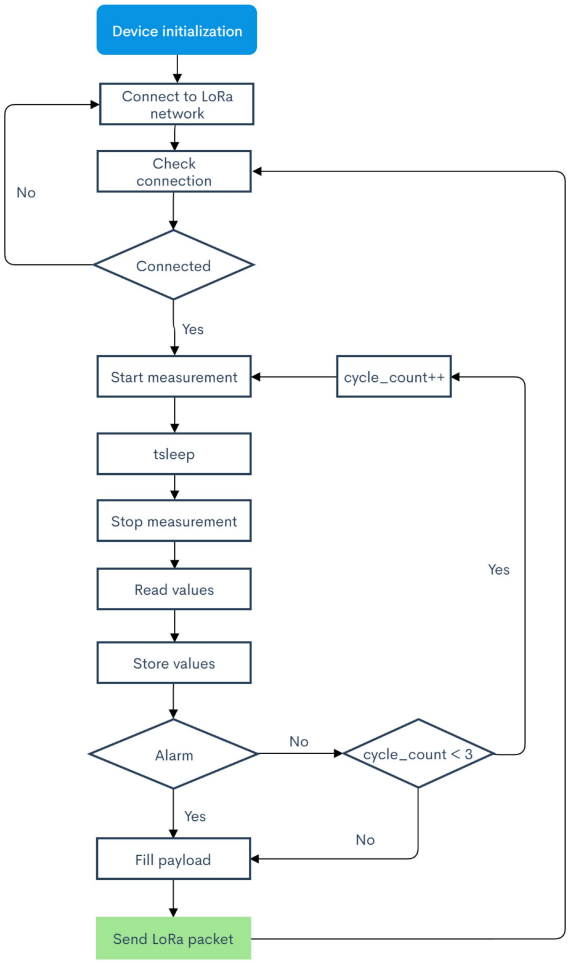

Fig. 8. Firmware data flowchart. The device enters in sleep mode while measuring for a certain time period designated as tsleep. This time interval depends on the configuration. For the power consumption measurements, tsleep was 120 s.

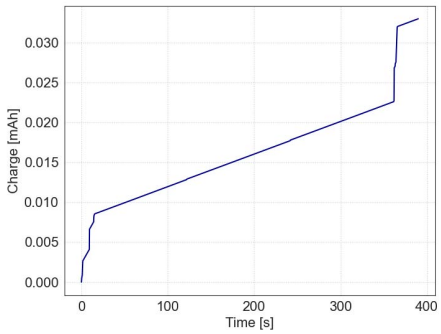

Fig. 9. Measured energy consumption of a customized D-shuttle LoRa node per 6-min duty cycle.

yet developed and the CERN LoRaWAN network was under deployment (see Section II-B). Therefore, the end devices consisted of a customized D-shuttle personal dosimeter properly modified to include both Wi-Fi and LoRa communication capabilities. The dosimeters were coupled to a Microchip RN2903 LoRa transceiver connected to an ESP32 board and an ANT-868-JJB-ST LoRa antenna. We identified the ESP32 Bluetooth Wi-Fi combo (Espressif Systems) as the best available option due to its high performances and ultralow power consumption. The communication boards were powered

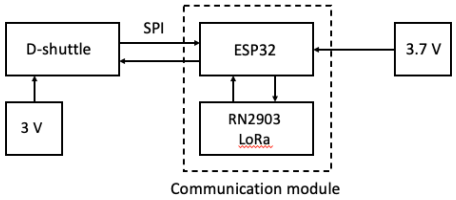

Fig. 10. Conceptual diagram of the master.

by a 3.7-V Li-ion rechargeable battery with a capacity of 3.4 Ah, while the radiation sensors were powered by a 3-V coin-type battery. A conceptual diagram of the master is shown in Fig. 10. For the slaves, we used the multiprotocol wireless module of the ESP32 board that provides Wi-Fi connectivity. Radiation measurements from the slaves were broadcasted synchronously to all the receivers in proximity, i.e., a slave does not synchronize its clock to the master but keeps sending the data until the data are received or the maximum attempt time of 60 s is exceeded [45]. In the same way, the Wi-Fi receiver of the master is ready to receive the data over 60 s. If after this time the communication is not established, the data packet is lost, and the slave needs to wait for the next scheduled transmission. This transmission method was chosen to avoid desynchronization among devices over time.

The configuration of the LoRa physical layer is summarized in Table II (Conf. 1) [46]. It is important to notice that the configuration of the LoRa physical layer has a direct impact on the communication range, sensitivity, energy efficiency, as well as packet reception efficiency [22], [47]–[49]. In this study, we used a bandwidth (BW) of 125 kHz, which is the narrowest BW value that can be set by the RN2903 module. Within this set of experiments, the chosen SF is 7. The SF that ranges from 7 to 12, is a key parameter in LoRaWAN and it is related to the data rate, i.e., number of chirps per second. The optimal value of the SF depends on the environmental conditions and affects the range of the transmission and the energy consumption. The aim of using an SF of 7 is to ensure the highest sensitivity and a low communication range. A higher SF, for example, an SF value of 12, will provide better coverage at the expense of increased power consumption. The frequency channel was set to the 868.5-MHz band and the transmission power to 14 dBm, which are the default values. The coding rate of a forward error correction code is the proportion of the transmitted data stream (bits) that is useful, and it is related to the time-on-air. The smaller the coding rate, the higher the time-on-air of the transmission. During our experiment, the coding rate was set to 4/5 and used by the LoRa modem to protect against interference.

In the container, each sensor was housed in a plastic waterproof box and protected by a light metal shield. The experiment lasted one week during which the container was emptied according to the standard garbage collection procedure. Data from the three slaves were broadcasted every hour via Wi-Fi to the master, which collected all the data and forwarded them to the database (IEEE 802.11 b/g/n protocol, frequency 2.4 GHz, up to 150 Mb/s). The master also embedded a radiation sensor. Similarly, data from the other four LoRa transceivers acting

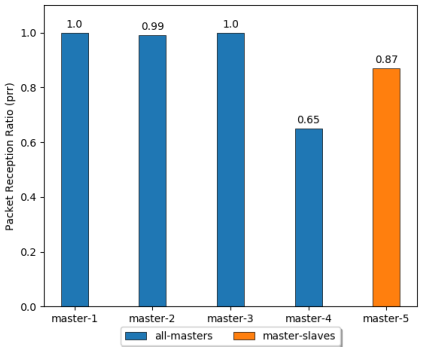

Fig. 11. PRR for the five masters, where master-5 is the device from the master–slaves configuration.

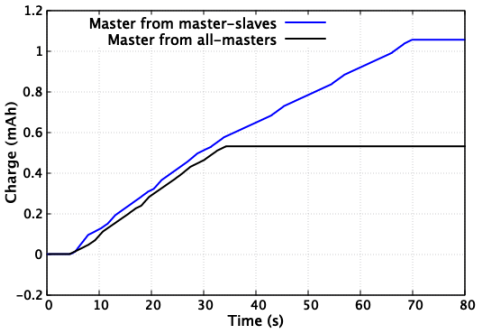

Fig. 12. Comparison between the measured energy consumption per cycle for a master device from the master–slaves model and an independent master (all-masters configuration).

as individual masters were sent every hour to the database. For the gateway, we used a MultiConnect Conduit model MTCDT-210A. At all times, the gateway was located indoors at a maximum distance of 50 m from the container. All devices were configured to send a 22-byte data packet every hour. Fig. 11 shows the prr of the five masters. The all-masters setup showed a high prr close to 1, except for one master that showed a lower transmission efficiency due to an unexpected battery voltage drop during the measurements. On the other hand, the master–slaves configuration experienced a packet loss of 13%, having a significant impact on the efficiency of the system due to the fact that when the master fails, no information from the entire container is registered until the next scheduled transmission. A faulty master in the all-masters configuration will have, on the other hand, a minimum impact on the monitoring system.

In addition to the data transfer efficiency, we also measured the power consumption of the different end devices. Results show that data transfer from the slaves to the master broadcasting a Wi-Fi signal is fast, leading to low power consumption, 93% less consuming than LoRa. Values were calculated over a full cycle, i.e., from deep-sleep to deep-sleep assuming one transmission per hour. However, since there is no synchronization between master and slaves, the slaves usually perform several attempts before the data are received by the master, entailing an increase in the final power consumption on both slaves and master. Fig. 12 shows the total energy consumption per cycle for the two types of masters. As can be seen, the energy consumption per cycle of an independent master is 0.5 mAh, instead of 1.05 mAh measured for the master in the master–slaves configuration. This is because the master in the master–slaves model needs more time to receive the data from all the slaves, read its own data, and transfer the different data packets consecutively to the LoRa server. This time difference is clearly visible in Fig. 12. Assuming a battery of nominal capacity of 2.5 Ah and one data transmission per hour, we would expect an increase of the master's battery lifetime of more than 100 days with respect to the master–slaves model (estimated battery lifetime of 204 days and 98 days, respectively). The results reported in this section showed that an all-masters configuration is a better solution. Moreover, with the new communication board (see Section III), the overall power consumption has been reduced to hundreds of μAh, allowing for a battery lifetime for the three types of sensors of around three years.

V. LoRa Experimental Range Test and Packet Reception Efficiency

We carried out a series of range tests to evaluate the LoRaWAN network coverage at CERN. The goal of the tests was to verify that the main areas where the waste containers are placed have good coverage with low interference, good building penetration, and low path loss, enabling high transmission efficiency with good signal quality and SNR. The packet reception efficiency inside and outside the metallic waste container was also evaluated. The results reported in this article have also been useful to assess the range and coverage of the CERN LoRaWAN network.

For this experiment, we used five NI-R02 radiation sensors. It should be noted that the performance of the LoRa signal is independent of the sensor, and therefore, similar results are expected with both the D-shuttle and the BG51 radiation sensors. For the measurements, we used the physical layer parameters as shown in Table II, with the settings reported in Conf. 2. Devices were programmed to transmit a 41-byte data packet every minute (30 bytes of sensor data) with a transmitting power of 14 dBm. Since the sensors are stationary with respect to the waste containers, which are in a relatively fixed position (variations of 50 m radius), the adaptive data rate (ADR) was enabled [50]. Moreover, the uplink messages were scattered over time in order to avoid the oversaturation of the network. The LoRaWAN configuration used during this experiment does not comply with the current frequency regulations of the CERN LoRaWAN network, which imposes a maximum of six uplink messages per hour. However, at the time of the test, only a few dozen devices were using the CERN LoRa network and our system did not increase the number of collisions. The final W-MON configuration is summarized in Table II Conf. 3, which implies a payload of 41 bytes sent every hour with ADR enabled. The data were directly collected from MQTT giving access to the packet payload, the received signal strength indicator (RSSI), and the SNR, as well as to the gateway information such as SF and coding rate.

The end devices were located at seven points around the CERN Meyrin site [see Fig. 3(a)]. The number and the position of the test points were decided based on various criteria, such

TABLE IV
DISTANCE IN METERS BETWEEN THE TEST POINTS AND THE LoRa GATEWAYS

Gateway	Test points						
	1	2	3	4	5	6	7
A	1200	900	1000	800	600	300	700
B	100	250	300	350	500	1300	1700
C	350	150	300	100	200	1000	1400
E	8100	8000	8400	8200	8000	7500	7000

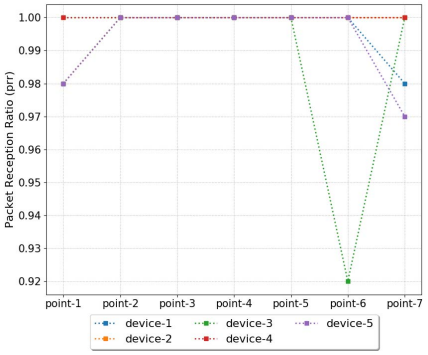

Fig. 13. PRR per device at the different test points.

as the actual position of the waste containers, the network coverage, and the relevance of the results. A similar test was carried out on the CERN Prévessin site, but the results are not reported in this article because of their similarity. Table IV summarizes the distance between the test points and the gateways. Gateway D is not included because it did not receive any uplink message during this specific study. The end devices were in a car during the tests. At each point, a minimum of 30 transmission attempts were carried out.

Fig. 13 summarizes the results of the data transfer obtained at the seven test points for the five end devices. As can be seen, the prr is overall very good with a success rate of 100% for almost all devices at the different test points. A slightly lower prr of 0.92 was measured for device 3 at test point 6 for no particular reason. A larger spread of the prr between devices was observed at point 7, at 700 m from the closest gateway, but the results remain acceptable with a prr above 0.97. It is worth mentioning that the occasional inefficiency in the data packet transmission is expected within the LoRaWAN standard. For W-MON, we use an ADR so that the end devices are able to automatically increase the SF if the transmission with a lower SF fails. Nonetheless, the frequency of the transmissions set to 1 m for this particular experiment is not optimal and can increase the number of collisions between devices dropping the number of receiving packages. This is of critical importance as the number of end devices significantly increases. During normal operation of the W-MON system, the devices are configured according to Conf. 3 in Table II, with a frequency of transmission of 1 h. This, together with the LoRa orthogonality [16], the ADR and the scattered of transmission over time, makes the collisions highly unlikely, even for a high number of devices.

Fig. 14 shows the average prr per gateway at the different test points. As expected, a higher success rate was obtained

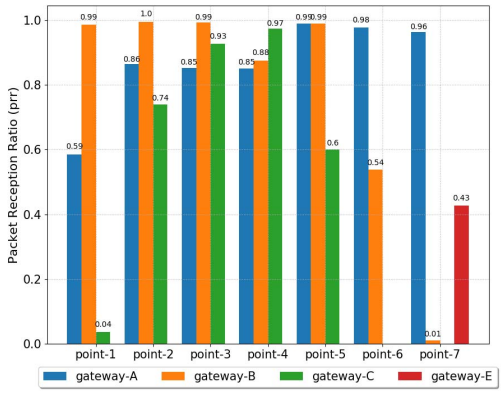

Fig. 14. Average prr of the different gateways at the seven test points.

when the distance to the gateway was reduced. For example, gateways located at less than 700 m from the devices presented a prr close to 1 (100% success rate). A prr below 0.6 was obtained for gateways located at more than 1 km. At distances between 700 m and 1 km, the success rate was 85%. This applies for both outdoor gateways A and B (see Table IV). The effect of outer and inner walls on the prr is illustrated in the results of gateway C. Gateway C, located inside the heavily shielded CERN High energy AcceleRator Mixed field/facility (CHARM) facility [51], had a prr close to 1 when the devices were close to the facility and with an open line of sight (no obstacles between the devices and the gateway). At points 1, 2, and 5, the prr was slightly lower due to the increased presence of building. At distances over 1 km, the loss probability significantly increases, being even of 100% for some cases. At point 7, located outside the CERN premises, the prr is close to 1 due to gateway A, placed at the highest point at CERN. Moreover, a few packets were surprisingly received by gateway E located at 7 km from the test point. Finally, the lower prr observed by the outdoor gateways at point 4 is due to the more dense urban environment that surrounded the end devices with a larger number of obstacles and buildings. It should be noted that in Fig. 14, some data packets were received by several gateways at the same time.

Besides the prr, the RSSI and the SNR were also analyzed [52]. Both RSSI and SNR are important parameters to determine the strength and quality of the LoRa signal and their evaluation can be very useful in the final deployment. Fig. 15(a) shows the average RSSI of all received packets per device at the seven test points for the closest outdoor gateway (gateway A for points 6 and 7 and gateway B for points 1–5) (gateways C–E were excluded from this analysis due to the very low prr at some of the test points). The average RSSI per device received by gateway B is shown in Fig. 15(b). Theoretically, the RSSI decreases as the distance between gateways and end devices increases. However, other parameters, such as the location and height of the gateway, the surroundings, and the weather conditions, should be considered when analyzing the RSSI [47], [53]. All the measurements reported here were conducted in similar weather and temperature conditions (mean temperature of 6 °C). In general, the higher the RSSI number, the stronger the LoRa signal (values closer to

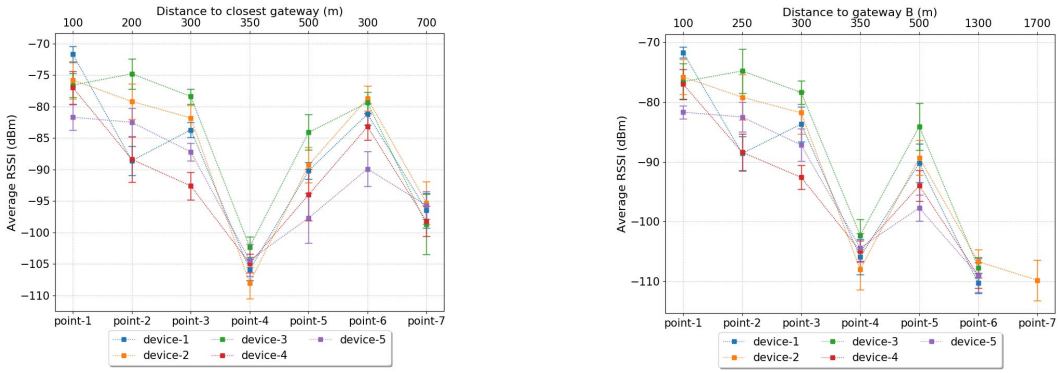

(a) (b)

Fig. 15. Average RSSI of all received packets per device at the seven measurement points for (a) closest gateway (excluding gateway C) and (b) gateway B.

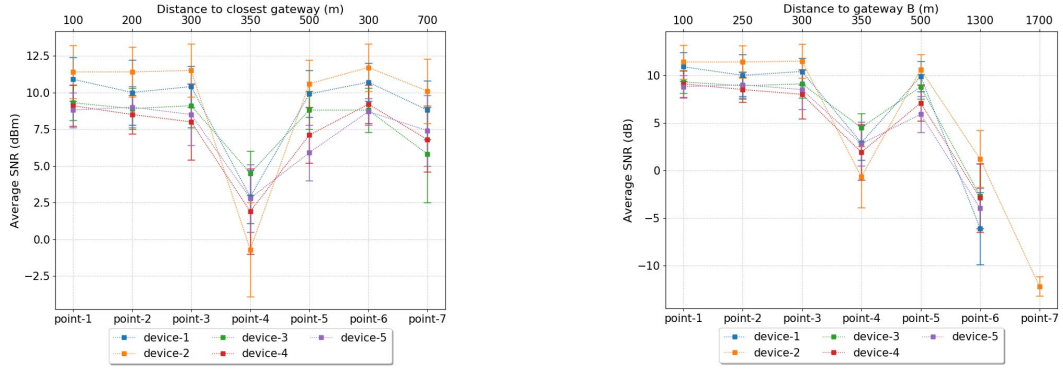

(a) (b)

Fig. 16. Average SNR of all received packets per device at the different test points for (a) closest gateway (excluding gateway C) and (b) gateway B.

0 indicate better signal strength). The results show that at all seven locations, the signals have a consistently good quality, with a mean RSSI value mostly greater than −95 dBm and a positive SNR. At distances above 1.3 km, the signals are received with an RSSI value between −106 and −110 dBm. At point 4, the signal strength dropped to −105 dBm due to the greater presence of obstacles and concrete buildings [see Fig. 15(a)]. The decrease of the RSSI with the distance is clearly visible in Fig. 15(b). As before, a lower expected RSSI value was measured at point 4. The SF was between 7 and 9 for all measurement points and five devices. Therefore, we can conclude that neither the RSSI values nor the SNR shows significant variations when changing the SF. We can see that the different locations do not have a big impact on the SNR, which is relatively constant at distances less than 700 m with a mean value close to 10 dB [see Fig. 16(a)], except at point 4 where a lower SRN of 2.5 dB was measured with no apparent effect on the prr. At farther distances over 1.3 km, the mean SNR value gets below 0 dB resulting in almost 100% packets lost [see Fig. 16(b)].

An additional test was carried out in order to evaluate the packet reception efficiency when the radiation sensors are installed inside and under a metallic container for ordinary waste. For this study, six NI-R02 radiation sensors configured according to Conf. 2 in Table II were placed for a minimum of 1 h at three different positions: inside, under, and outside (on top) of one of the containers placed at point 3 (see Fig. 3 and Table IV). As expected, a packet reception efficiency of 100% was measured with the devices placed outside and on top of the container. A reduction of around 10% and 12% was obtained with the radiation sensors placed inside and under the container, respectively. It can be concluded from these tests that the Meyrin site at CERN has a good LoRa coverage up to 1.7 km with a good signal quality and a packet reception efficiency of approximately 90% being suitable for the W-MON application.

VI. Conclusion

This article presents the implementation of an interconnected network of gamma radiation sensors for an IoT-based environmental radiation monitoring system. The first implementation of an IoT LoRaWAN distributed network for real-time remote monitoring of radioactivity in metallic waste containers is presented in this article. The effects of a metallic container on the LoRa packet reception efficiency are also evaluated for the first time. The end device consists of a highly sensitive and compact gamma radiation sensor coupled to an ultralow-power electronic board with custom-designed hardware and software for long-range low-power LoRa wireless data transmission. The end devices are installed in metallic containers for ordinary waste in sets of eight devices per container, offering continuous monitoring of the radiation levels

inside the containers, providing identification and early warning of a possible radiation release event, and thus overcoming the limitations posed by the manual radiological controls. The radiation measurements are periodically sent to the CERN LNS that includes ten outdoor and one indoor gateways. The network coverage, signal quality, SNR, as well as packet reception efficiency have been evaluated within the scope of the W-MON project. For these tests, we used five end devices placed at seven different locations around the CERN Meyrin site. The devices were in a car during the tests. Results showed that all areas where the waste containers are placed have a high coverage range with low interference and packet lost. A loss in the prr of 10% and 12% is foreseen when installing the end device inside and under the containers. Real-time monitoring, data visualization, data storage, data processing, status control of the devices, and alarm notification are possible due to a robust and reliable end-to-end data infrastructure that has been developed before the final integration into REMUS, the overall CERN REMUS.

The current W-MON pilot network includes three waste containers with a total of 24 nodes (eight sensors per container) sending data every hour to the network. Three different types of radiation sensor are currently under investigation, and hence, each container has been equipped with a specific type of device. The three containers will be operational for several months and subjected to real operational conditions. The scope of the tests is to evaluate the performance of the three dosimeters over a long time period in terms of sensitivity, power consumption, data transmission efficiency, robustness, stability, and reliability, to evaluate the capability as an environmental radiation monitoring system, establish the detection limit for the radiological classification of potentially radioactive items, and implement the detection criteria into REMUS.

ACKNOWLEDGMENT

The authors would like to thank the European Organization for Nuclear Research (CERN) IT-CS and IT-DB groups for their technical guidance and assistance, H. Odziemczyk (CERN) for his advice and help during the LoRa efficiency tests, N. Matos de Barros (CERN) for his support and assistance with the development of the data pipeline architecture, and G. Ducos (CERN) for his help in the performance tests.

REFERENCES

[1] L. Gallego Manzano *et al.*, "A distributed and interconnected network of sensors for environmental radiological monitoring," *Radiat. Meas.*, vol. 139, Dec. 2020, Art. no. 106488. [Online]. Available: http://www.sciencedirect.com/science/article/pii/S1350448720302626

[2] B.-Y. Ooi and S. Shirmohammadi, "The potential of IoT for instrumentation and measurement," *IEEE Instrum. Meas. Mag.*, vol. 23, no. 3, pp. 21–26, May 2020.

[3] Y. Cai, A. Genovese, V. Piuri, F. Scotti, and M. Siegel, "IoT-based architectures for sensing and local data processing in ambient intelligence: Research and industrial trends," in *Proc. IEEE Int. Instrum. Meas. Technol. Conf. (I2MTC)*, May 2019, pp. 1–6.

[4] R. O. Andrade and S. G. Yoo, "A comprehensive study of the use of LoRa in the development of smart cities," *Appl. Sci.*, vol. 9, no. 22, p. 4753, Nov. 2019.

[5] J. Jaime, I. Sousa, M. P. Queluz, and A. Rodrigues, "Planning a smart city sensor network based on LoRaWAN technology," in *Proc. 21st Int. Symp. Wireless Pers. Multimedia Commun. (WPMC)*, Nov. 2018, pp. 35–40.

[6] C. Scuro, P. Sciammarella, F. Lamonaca, R. Olivito, and D. Carnì, "IoT for structural health monitoring," *IEEE Instrum. Meas. Mag.*, vol. 21, no. 6, pp. 4–9, Dec. 2018.

[7] G. Mois, S. Folea, and T. Sanislav, "Analysis of three IoT-based wireless sensors for environmental monitoring," *IEEE Trans. Instrum. Meas.*, vol. 66, no. 8, pp. 2056–2064, Aug. 2017.

[8] G. Mois, T. Sanislav, and S. C. Folea, "A cyber-physical system for environmental monitoring," *IEEE Trans. Instrum. Meas.*, vol. 65, no. 6, pp. 1463–1471, Jun. 2016.

[9] A. I. Sunny, A. Zhao, L. Li, and S. K. K. Sakiliba, "Low-cost IoT-based sensor system: A case study on harsh environmental monitoring," *Sensors*, vol. 21, no. 1, p. 214, Dec. 2020, doi: 10.3390/s21010214.

[10] C.-Y. Chung, I.-T. Peng, and J.-C. Yeh, "Environmental monitoring and smart garbage sorting system based on LoRa wireless transmission technology," in *Proc. IEEE 2nd Eurasia Conf. Biomed. Eng., Healthcare Sustainability (ECBIOS)*, May 2020, pp. 43–46.

[11] T. J. Sheng *et al.*, "An Internet of Things based smart waste management system using LoRa and tensorflow deep learning model," *IEEE Access*, vol. 8, pp. 148793–148811, 2020.

[12] M. Cerchecci, F. Luti, A. Mecocci, S. Parrino, G. Peruzzi, and A. Pozzebon, "A low power IoT sensor node architecture for waste management within smart cities context," *Sensors*, vol. 18, no. 4, p. 1282, Apr. 2018, doi: 10.3390/s18041282.

[13] R. Gomaa, I. Adly, K. Sharshar, A. Safwat, and H. Ragai, "ZigBee wireless sensor network for radiation monitoring at nuclear facilities," in *Proc. 6th Joint IFIP Wireless Mobile Netw. Conf. (WMNC)*, Apr. 2013, pp. 1–4.

[14] J. Ebenezer and S. S. Murty, "Deployment of wireless sensor network for radiation monitoring," in *Proc. Int. Conf. Comput. Netw. Commun. (CoCoNet)*, Dec. 2015, pp. 27–32.

[15] H.-C. Lee and K.-H. Ke, "Monitoring of large-area IoT sensors using a LoRa wireless mesh network system: Design and evaluation," *IEEE Trans. Instrum. Meas.*, vol. 67, no. 9, pp. 2177–2187, Sep. 2018.

[16] (2020). *LoRa Alliance*. Accessed: Apr. 20, 2020. [Online]. Available: https://lora-alliance.org/about-lorawan

[17] A. Ledeul, G. Segura, R.-P. Silvola, B. Styczen, and D. V. Ribeira, "REMUS: The new CERN radiation and environment monitoring unified supervision," in *Proc. ICALEPCS*, Melbourne, VIC, Australia, 2015, Art. no. TUD3O03.

[18] U. Raza, P. Kulkarni, and M. Sooriyabandara, "Low power wide area networks: An overview," *IEEE Commun. Surveys Tuts.*, vol. 19, no. 2, pp. 855–873, 2nd Quart., 2017.

[19] B. Moyer, "Low power, wide area: A survey of longer-range IoT wireless protocols," *Electron. Eng. J.*, 2015. [Online]. Available: http://www.eejournal.com/archives/articles/20150907-lpwa/

[20] A. Augustin, J. Yi, T. Clausen, and W. Townsley, "A study of LoRa: Long range & low power networks for the Internet of Things," *Sensors*, vol. 16, no. 9, p. 1466, Sep. 2016.

[21] J. Petäjäjärvi, K. Mikhaylov, M. Pettissalo, J. Janhunen, and J. Iinatti, "Performance of a low-power wide-area network based on LoRa technology: Doppler robustness, scalability, and coverage," *Int. J. Distrib. Sensor Netw.*, vol. 13, pp. 1–16, Mar. 2017.

[22] S. Kartakis, B. D. Choudhary, A. D. Gluhak, L. Lambrinos, and J. A. McCann, "Demystifying low-power wide-area communications for city IoT applications," in *Proc. 10th ACM Int. Workshop Wireless Netw. Testbeds, Experim. Eval., Characterization*, Oct. 2016, pp. 2–8.

[23] A. Rahmadhani and F. Kuipers. (2017). *Understanding Collisions in a LoRaWAN*. [Online]. Available: https://wiki.surfnet.nl/download/attachments/60702138/TUD-LoRaWAN-RoN%-2017.pdf

[24] M. C. Bor, U. Roedig, T. Voigt, and J. M. Alonso, "Do LoRa low-power wide-area networks scale?" in *Proc. 19th ACM Int. Conf. Modeling, Anal. Simulation Wireless Mobile Syst.*, Nov. 2016, pp. 59–67, doi: 10.1145/2988287.2989163.

[25] O. Georgiou and U. Raza, "Low power wide area network analysis: Can LoRa scale?" *IEEE Wireless Commun. Lett.*, vol. 6, no. 2, pp. 162–165, Apr. 2017.

[26] T. Voigt, M. Bor, U. Roedig, and J. Alonso, "Mitigating inter-network interference in LoRa networks," in *Proc. 2nd Int. Workshop New Wireless Commun. Paradigms Internet Things (MadCom)*, 2017, pp. 20–22.

[27] R. Singh, R. Berkvens, and M. Weyn, "Time synchronization with channel hopping scheme for LoRa networks," in *Advances on P2P, Parallel, Grid, Cloud and Internet Computing*. Cham, Switzerland: Springer, Jan. 2020, pp. 786–797.

[28] D. Camps-Mur, A. Garcia-Saavedra, and P. Serrano, "Device-to-device communications with Wi-Fi direct: Overview and experimentation," *IEEE Wireless Commun.*, vol. 20, no. 3, pp. 96–104, Jun. 2013.
[29] J.-S. Lee, Y.-W. Su, and C.-C. Shen, "A comparative study of wireless protocols: Bluetooth, UWB, ZigBee, and Wi-Fi," in *Proc. IECON 33rd Annu. Conf. IEEE Ind. Electron. Soc.*, Nov. 2007, pp. 46–51.
[30] *ChirpStack: Open-Source LoRaWAN Network Server*. Accessed: Nov. 6, 2020. [Online]. Available: https://www.chirpstack.io/
[31] *MQTT: The Standard for IoT Messaging*. Accessed: Nov. 2, 2020. [Online]. Available: http://mqtt.org/
[32] *Apache Kafka*. Accessed: Nov. 2, 2020. [Online]. Available: https://kafka.apache.org/
[33] *InfluxDB*. Accessed: Nov. 2, 2020. [Online]. Available: https://www.influxdata.com/
[34] *Grafana*. Accessed: Nov. 2, 2020. [Online]. Available: https://grafana.com/
[35] V. A. Dambal, S. Mohadikar, A. Kumbhar, and I. Guvenc, "Improving LoRa signal coverage in urban and sub-urban environments with UAVs," in *Proc. Int. Workshop Antenna Technol. (iWAT)*, Mar. 2019, pp. 210–213.
[36] J. Haxhibeqiri, A. Karaagac, F. Van den Abeele, W. Joseph, I. Moerman, and J. Hoebeke, "LoRa indoor coverage and performance in an industrial environment: Case study," in *Proc. 22nd IEEE Int. Conf. Emerg. Technol. Factory Autom. (ETFA)*, Sep. 2017, pp. 1–8.
[37] M. Bor, J. Vidler, and U. Roedig, "LoRa for the Internet of Things," in *Proc. EWSN*, Feb. 2016, pp. 361–366.
[38] O. Iova *et al.*, "LoRa from the city to the mountains: Exploration of hardware and environmental factors," in *Proc. Int. Conf. Embedded Wireless Syst. Netw. (EWSN)*. Uppsala, Sweden: Uppsala Univ., Feb. 2017, pp. 317–322. [Online]. Available: http://hdl.handle.net/10449/42132
[39] R. Sanchez-Iborra, I. G. Liaño, C. Simoes, E. Couñago, and A. Skarmeta, "Tracking and monitoring system based on LoRa technology for lightweight boats," *Electronics*, vol. 8, no. 1, p. 15, Dec. 2018.
[40] L. Li, J. Ren, and Q. Zhu, "On the application of LoRa LPWAN technology in sailing monitoring system," in *Proc. 13th Annu. Conf. Wireless Demand Netw. Syst. Services (WONS)*, Feb. 2017, pp. 77–80.
[41] R. Sierra, "Put a sensor in your life with the new LoRaWAN network," Bull. CERN Community, Geneva, Switzerland, Tech. Rep. 5-6/2019, 2019.
[42] S. Danzeca, "A radiation tolerant wireless Internet of Things (IoT) platform for on-field sensor data acquisition," presented at the CERN ATS-KT Innov. Day, 2018. [Online]. Available: https://indico.cern.ch/event/752949/contributions/3183928/attachments/1742219/2819246/A_radiation_tolerant_wireless_Internet_of_Things_IoT_platform_for_on-field_sensor_data_acquisition_Salvatore_Danzeca_final.pdf
[43] F. Pozzi *et al.*, "CERN irradiation facilities," *Radiat. Protection Dosimetry*, vol. 180, nos. 1–4, pp. 120–124, Aug. 2018.
[44] F. Pozzi, "CERN radiation protection (RP) calibration facilities," Ph.D. dissertation, CERN Radiat. Protection Group, Technischen Universität München, Munich, Germany, 2016.
[45] H. Seongmin, L. Jihyung, and L. Kyunghan, "QuickTalk: An association-free communication method for IoT devices in proximity," *Proc. ACM Interact., Mobile, Wearable Ubiquitous Technol.*, vol. 1, no. 3, pp. 56:1–56:18, 2017.
[46] (2015). *Semtech. LoRaWAN Specification v1.0.3*. Accessed: Jun. 22, 2020. [Online]. Available: https://lora-alliance.org/resource-hub/lorawanr-specification-v103
[47] M. Cattani, C. Boano, and K. Römer, "An experimental evaluation of the reliability of LoRa long-range low-power wireless communication," *J. Sensor Actuator Netw.*, vol. 6, no. 2, p. 7, Jun. 2017.
[48] T. Attia, M. Heusse, B. Tourancheau, and A. Duda, "Experimental characterization of LoRaWAN link quality," in *Proc. IEEE Global Commun. Conf. (GLOBECOM)*, Dec. 2019, pp. 1–6.
[49] R. Sanchez-Iborra, J. Sanchez-Gomez, J. Ballesta-Viñas, M.-D. Cano, and A. Skarmeta, "Performance evaluation of LoRa considering scenario conditions," *Sensors*, vol. 18, no. 3, p. 772, Mar. 2018.
[50] *LoRaWAN Adaptive Data Rate*. Accessed: Nov. 17, 2020. [Online]. Available: https://www.thethingsnetwork.org/docs/lorawan/adaptive-data-rate.html%
[51] J. Mekki, M. Brugger, R. G. Alia, A. Thornton, N. C. D. S. Mota, and S. Danzeca, "CHARM: A mixed field facility at CERN for radiation tests in ground, atmospheric, space and accelerator representative environments," *IEEE Trans. Nucl. Sci.*, vol. 63, no. 4, pp. 2106–2114, Aug. 2016.
[52] Z. A. Tan *et al.*, "Analysis on LoRa RSSI in urban, sub-urban, and rural area for handover signal strength-based algorithm," *IOP Conf. Ser., Mater. Sci. Eng.*, vol. 705, Dec. 2019, Art. no. 012012.
[53] H. Wennerstrom, F. Hermans, O. Rensfelt, C. Rohner, and L.-A. Norden, "A long-term study of correlations between meteorological conditions and 802.15.4 link performance," in *Proc. IEEE Int. Conf. Sens., Commun. Netw. (SECON)*, Jun. 2013, pp. 221–229.

L. Gallego Manzano was born in Spain, in 1986. She received the B.S. degree in fundamental physics and the M.S. degree in biomedical physics from the University Complutense of Madrid, Madrid, Spain, in 2010 and 2011, respectively, and the Ph.D. degree in experimental nuclear physics from the Subatech Laboratory and IMT Atlantique, Nantes, France, in 2016.

In 2012, she was a Research Assistant with the Department of Atomic, Molecular and Nuclear Physics, University Complutense of Madrid. From 2016 to 2017, she was the Operations Manager of the XEMIS2 liquid xenon facility at Subatech Laboratory. From 2017 to 2020, she worked as a Senior Post-Doctoral Researcher with the Radiation Protection Group, European Organization for Nuclear Research (CERN), Meyrin, Switzerland. In 2020, she joined the Institute of Radiation Physics, Lausanne University Hospital, Lausanne, Switzerland. Since 2021, she has been the Project Leader of the European MARS Collaboration at Lausanne University Hospital. She also works as a Cooperation Associate with the CERN Radiation Protection Group. Her research interests include detector development, dosimetry, radiation protection, and medical imaging.

Dr. Manzano was a recipient of the NIM-A Young Scientist Award in 2017.

Hamza Boukabache (Member, IEEE) received the master's degree in electronic and automatic control from the National Institute of Applied Science of Toulouse, Toulouse, France, in 2009, the master's degree in microtechnology from the University of Toulouse, Toulouse, in 2009, and the Ph.D. degree in microsystem and nanosystem from the National Institute of Applied Sciences of Toulouse in 2013.

He is currently the Project Leader with the Radiation Protection Group, European Organization for Nuclear Research (CERN), Geneva, Switzerland, leading a team in charge of the development and manufacturing of a new-generation ionizing radiation monitoring system. His research interests include system-on-chip development, ultralow current measurement techniques, and hardening methods for safety critical systems.

Dr. Boukabache has received many awards for his research work in heterogeneous aerospace structural health monitoring within the French National Center for Scientific Research (CNRS). He was a recipient of the Engineering Sciences Prize from the Toulouse Academy of Science in 2014 and the GEET Prize in 2013 for the best Ph.D. research work among five universities and nominated the same year for the sixth top innovations in French aerospace cluster.

Salvatore Danzeca received the Ph.D. degree from the University of Montpellier, Montpellier, France, in 2015, after carrying out his studies at the European Organization for Nuclear Research (CERN), Geneva, Switzerland.

His work was performed in the context of the Radiation to Electronic Project (R2E) and focused on the characterization and the qualification of the radiation sensors to embed on the Radiation Monitor (RadMon) for the electronics found in the CERN accelerators. He is currently the Section Leader of the Radiation Tolerant and Measurement Electronics Team, CERN, which is a section that includes 15 people. He is responsible for the operation, monitoring, and maintenance of more than 500 RadMon installed in the large hadron collider (LHC) and in the injectors chain. He is also responsible for two radiation test facilities at CERN: CC60 (a Co60 facility) and CERN High energy AcceleRator Mixed field/facility (CHARM). In addition, he handles the radiation testing and qualification service for COTS components in the context of CERN applications.

Dr. Danzeca is also the Chairman of the RADiation Working Group (RADWG), which provides support to the accelerator sector equipment groups for the assessment of the radiation tolerance of electronic equipment to be installed in radiation-exposed areas.

Natalie Heracleous received the Doctorate of Philosophy (Ph.D.) degree in elementary particle physics from RWTH Aachen University, Aachen, Germany, in 2013.

She was a member of the CMS Collaboration at the European Organization for Nuclear Research (CERN), Geneva, Switzerland, for more than eight years. She is currently a Physicist. She has substantial experience in dealing with big and complex data and participated in a variety of physics analyses using particle collision data as well as in detector development projects. For the last four years, she performs her research at the CERN Radiation Protection Group on detector applications for medical and protection purposes.

Fabrizio Murtas was born in Rome, Italy, in 1962. He received the B.S. degree in particle physics from the Università La Sapienza, Rome, Italy, in 1988.

Since 1993, he has been a Staff Researcher with Frascati National Laboratories, Italian Institute for Nuclear Physics (INFN), Frascati, Italy. From 2012 to 2015, he was a Scientific Associate with the European Organization for Nuclear Research (CERN), Geneva, Switzerland. Since 2015, he has been a Project Associate with the Radiation Protection Group, CERN. He was the Director of INFN Scientific Database Service from 2003 to 2012 and the responsible for the INFN Research Office until 2012. His research interests include high-energy physics, calorimetry, muon chambers, neutron detectors, and dosimetry. He has collaborated in numerous international experiments: ALEPH (CERN), KLOE (LNF-INFN), MONOLITH (Gran Sasso), LHCb (CERN), UA9 (CERN), and n TOF (CERN). Since the past years, he has been responsible for the INFN Research and Development activity dedicated to the applications of gas electron multipliers (GEMs). He has developed numerous novel GEM-based detectors for applications in particle and medical physics and dosimetry. He has a worldwide known and appreciated expertise in the detector field, being a referee of international publications.

Daniel Perrin was born in France, in 1963. He received the Diploma degree in electronics from the University Institute of Technology, Saint Étienne, France, in 1983.

After his Diploma degree, he worked at the European Organization for Nuclear Research (CERN), Geneva, Switzerland, as an Electronics Technical Engineer, in developing the control units of the electrostatic separators for the large electron–positron (LEP) collider. In 1992, he joined the CERN Radiation Protection Group, for which he designed and developed instrumentation for ionizing radiation measurement. Since 2001, he has been the Head of the CERN Radiation Protection Group, Instrumentation and Logistics Section. He has led projects on the design and supply of the radiation monitoring system for the large hadron collider (LHC) and the injector chain. Since 2013, he has been managing the Radiation Monitoring System for the Environment and Safety (RAMSES) Program at CERN.

Vasja Pirc was born in Slovenia, in 1998. He is currently studying electronics engineering at the University of Maribor, Maribor, Slovenia.

He was an Intern at the European Organization for Nuclear Research (CERN), Geneva, Switzerland, from 2020 to 2021.

Alejandro Ribagorda Alfaro received the bachelor's degree in electronics and automation engineering from the Polytechnic University of Albacete, Albacete, Spain, in 2019.

From 2019 to 2020, he was a Trainee with the European Organization for Nuclear Research (CERN), Meyrin, Switzerland, on the development of embedded firmware for environmental radiation monitoring. Since 2020, he has been working as a LabView Control System Engineer at the Fast Accelerator Control System Group, Advanced Oncotherapy plc, Meyrin.

Mr. Alfaro was a recipient of the Final Degree Project Award from the region of Castilla-La Mancha, Spain, in 2019, with a real-time sign language interpreter system in Android. In 2017, he was recognized as one of the Top 5 World- NASA Space Apps in the Category "Most Inspiring."

Alessandro Zimmaro was born in Italy, in 1994. He received the M.Sc. degree in electronic engineering from the University of Federico II of Naples, Naples, Italy, in 2020. He is currently pursuing the Ph.D. degree in system-level testing under radiation with the University of Montpellier, Montpellier, France, and the European Organization for Nuclear Research (CERN), Geneva, Switzerland.

He has been with CERN since 2019.

Marco Silari graduated in physics from the University of Milan, Milan, Italy, in 1982. He received the Ph.D. degree in medical physics from the University of Milan in 1985.

From 1984 to 1995, he was a Researcher with the Italian National Research Council (CNR), Milan. He spent the first two years of this period as a Visiting Scientist at the Medical Research Council (MRC) Cyclotron Unit, Hammersmith Hospital, London, U.K., where he worked on the installation of a 40-MeV proton medical cyclotron. From 1991 to 1995, he worked with Prof. Ugo Amaldi on the Italian Hadrontherapy Project, where he was the Project Leader for the National Centre for Oncological Hadrontherapy (CNAO), which in 2011 started patient treatments in Pavia, near Milan. He has been with the European Organization for Nuclear Research (CERN), Geneva, Switzerland, as a Staff Member since 1996 and a Senior Physicist since 2001. Within the Radiation Protection (RP) Group, over the years, he has led various sections of the RP group with responsibility for radiation protection around the SPS, PS, and LEP accelerators, radiation protection of LEP decommissioning, and for radiation protection studies of the large hadron collider (LHC) experiments and future CERN accelerators. He is now leading the Special Projects Section, whose activities include detector research and development and radiological characterization of materials for their free release in Switzerland. He was a scientist-in-charge of the EU Marie Curie projects RADENV from 2006 to 2009 on accelerator radiation protection and ARDENT from 2012 to 2016 on advanced radiation dosimetry. Throughout the years, he has maintained a keen interest in medical physics and an academic interest as a supervisor of many master and Ph.D. students. He has taught for 13 years at the Ph.D. School of Medical Physics, Milan. He is the author of more than 190 scientific publications and holds two patents.

Dr. Silari has been a member of two working groups of EURADOS and the EURADOS Council since January 2020.